REPORT No. 76

CONDENSATION OF CARBON DIOXIDE IN SUPERSONIC NOZZLES

KARL M. DUFF

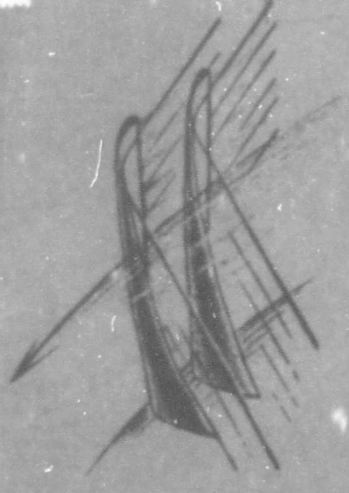

September, 1964

GAS TURBINE LABORATORY
MASSACHUSETTS INSTITUTE OF TECHNOLOGY
CAMBRIDGE · 39 · MASSACHUSETTS

ABSTRACT

Condensation of CO_2 in a supersonic nozzle is investigated. Descriptions of test apparatus and nozzle are presented along with data and plotted pressure profiles for both condensing and non-condensing CO_2. Limited comparison of theoretical and experimental methods is inconclusive, but suggests that the homogeneous nucleation theory is valid for the condensation of CO_2. Limited results of density measurements by means of the interferometer are presented and the difficulties encountered in employing this instrument are discussed. Finally, recommendations for resolving these difficulties and for further efforts in this investigation are suggested.

CONDENSATION OF CARBON DIOXIDE IN SUPERSONIC NOZZLES

by

Karl M. Duff

Research was carried out under the
Sponsorship of U.S. Navy, Office
of Naval Research, Power Branch
Contract Nonr 3963(07)

GAS TURBINE LABORATORY
REPORT No. 76

September 1964

MASSACHUSETTS INSTITUTE OF TECHNOLOGY
Cambridge, Massachusetts

ABSTRACT

Condensation of CO_2 in a supersonic nozzle is investigated. Descriptions of test apparatus and nozzle are presented along with data and plotted pressure profiles for both condensing and non-condensing CO_2. Limited comparison of theoretical and experimental methods is inconclusive, but suggests that the homogeneous nucleation theory is valid for the condensation of CO_2. Limited results of density measurements by means of the interferometer are presented and the difficulties encountered in employing this instrument are discussed. Finally, recommendations for resolving these difficulties and for further efforts in this investigation are suggested.

Test results indicate a definite region of supersaturation of CO_2 prior to its expansion. In Curve I, using assumed

isentropic temperatures based on measured pressure ratio, the supersaturation ratio (ratio of static pressure to flat-surface equilibrium pressure at local temperature) obtains an estimated value of 9.14, prior to condensation occurring.

~~In this expression P_∞ is the pressure at which a flat surfaced liquid would remain at equilibrium with its vapor, at the temperature of the environment.~~

In Curve 3, the supersaturation ratio reaches a value of 10.5 prior to condensation and in Curves 4, 5 and 7 values of 11.6, 13.4 and 16.8, respectively. ~~Calculations~~ of these figures are ~~in Appendix D.~~

The fact that supersaturation ratios steadily increase prior to the occurence of rapid condensation tends to support the predictions of nucleation theory that, for CO_2, the lines of constant nucleation rate diverge with decreasing pressure and temperatures and that nucleation rates have a critical value of the ratio between the static and stagnation pressures beyond which they rise astronomically, creating a narrow zone where the large portion of condensation occurs. ~~The nucleation rates predicted by equation a(1) in Appendix B are shown in Fig. 12, and indicate that a greater supersaturation is required at lower temperatures to obtain a given nucleation rate.~~

~~However, in the absence of more complete testing of the combination of nucleation, drop growth, and gas dynamic theory, little more can be said at present.~~

It is further concluded that the interferometer does not lend itself to the convenient procurement of accurate density and pressure profiles in this particular nozzle under these extreme temperature conditions. The degree of accuracy in profiles obtained, however, in the absence of any corrective procedures, provides a reasonable hope that simple correction procedures can be applied to increase the interferometer's accuracy and usefulness for this study.

The fact that interference fringes in the interferometer photos remain nearly verticle at all regions of the nozzle until the boundary layer is

ACKNOWLEDGEMENTS

The author gratefully acknowledges the contributions of Professor Philip G. Hill, thesis supervisor, who first suggested this work and whose advice and encouragement were of great help, Mr. Michael Kremmer, who along with Prof. Hill programmed the basic theoretical equations involved in the study for use at the M.I.T. computer center, and Messrs. Dalton Baugh and Thorwald Christiansen and staff who were invaluable in their construction of and modifications to the test apparatus.

He is also indebted to Mrs. Gretchen Durf who typed the rough and final manuscripts, Mr. John Macrae who assisted in the drawing of curves, and Mrs. Madelyn Euvrard who lent great assistance in advice and materials throughout the research and in its final publication.

TABLE OF CONTENTS

NOMENCLATURE

A .... Nozzle Cross-sectional Area

A* .... Nozzle Throat Area

b .... Nozzle Height, inches

C_p .... Specific Heat at Constant Pressure BTU/lbm °F

G .... Gladstone-Dale Constant - $.3673 \times 10^{-2}$ for CO_2

h_{fg}.... Heat of Vaporization BTU/lbm

J .... Nucleation Rate - nuclei/ft^3 sec.

k .... Ratio of Specific Heats, C_p/C_v

K .... Boltzmann Constant

l .... Nozzle width (Distance between plates, .956")

λ_o .... Wave Length of Interferometer Light Source, 5461a°

M .... Mach Number

μ .... Mass Fraction of Moisture Present in Vapor

n .... Index of Refraction, C_o/C

P .... Static Pressure, as noted

P_o .... Stagnation Pressure

P_∞.... Flat Surface Equilibrium Pressure at Local Temperature

P_* .... Throat Pressure

ρ .... Static Density, lbm/ft^3

ρ_o .... Stagnation Density, lbm/ft^3

r .... Drop Radius

S .... Interferometric Fringe Shift, number of fringes

σ .... Drop Surface Tension

τ .... Time Constant, seconds

T .... Static Temperature, ^oR

T_o .... Stagnation Temperature, ^oR

x .... Distance along Nozzle, inches

I. INTRODUCTION

Despite extensive theoretical work in the field of homogeneous nucleation and condensation, there exists considerable divergence in the predicted nucleation and condensation rates of many authors. Many so-called "corrections" to the theory have been contributed in recent years, which have only served to further cloud an already involved theoretical picture of the homogeneous nucleation and condensation process. The problem will remain unresolved until the meager amount of existing experimental data in the field is supplemented by further work involving a variety of gases extensive enough to thoroughly test the theory and determine exactly what the important parameters and their influences are.

Volmer and Flood[20] first did extensive cloud chamber experimentation on a variety of vapors, effectively determining the "critical" supersaturation ratios of these gases, beyond which condensation occurred extremely rapidly. This data has been considerably overworked in attempts to extrapolate other data, such as condensation rates, etc., from it. Later, Binnie and Green[3] and others measured condensation of steam in supersonic nozzles, and some limited data on nitrogen has been presented by Willmarth and Nagamatsu,[23] and Faro, Small and Hill.[7] More recently, Wegener[21] has been doing extensive experimentation with humidified air in supersonic nozzles and has concluded that predicted nucleation rates of various authors[1,20,24] are incorrect.

The work presented here was undertaken to attempt to help resolve the problem described above by study of condensation in additional, as yet untested, vapors. The problem is particularly pertinent regarding flow in nozzles, since recent proposed work on space power plants has involved turbines using such vapors as sodium, potassium and rubidium, or other vapors about which insufficient knowledge exists on which to base the design of such turbines.

In the experimental investigation of homogeneous nucleation and condensation, the use of a sudden expansion by means of a supersonic nozzle recommends itself for several reasons, though numerous other methods of producing condensation exist. As compared to other methods of expansion, a supersonic nozzle allows a maximum relaxation rate in the simplest possible manner. This is necessary in order to produce supersaturation to a maximum degree and to provide a proper basis on which to test nucleation theory.

A nozzle expansion further allows convenient quantitative measurement of the gas properties at all stages of the expansion, including the stagnation conditions. In the region of condensation, measurement of the gas properties also provides a means of determining the rates and amounts of condensation at each point. This study employed the use of static pressure measurements, which have been shown by Binnie and Green[3] and others previously mentioned to be a sensitive indicator of the heat released by condensation. Measurement of gas density through the use of the interferometer was also employed here in an effort to quantitatively study condensation in nozzles.

II. DESCRIPTION OF APPARATUS AND TEST PROCEDURES

The schematic arrangement of the test apparatus is shown in Fig. 1. A manifold connected nine 50 lb. CO_2 cylinders and led to a needle valve which was used as a regulator of gas flow to the stagnation tank and nozzle. Nozzle exhaust was to atmosphere.

The stagnation tank was fitted with a removable end plate which allowed placing a large filter bag containing activated granules of charcoal between layers of fiber glass into the stagnation tank. This filter was intended to limit the passage of foreign particules into the nozzle and also served as a heat source, decreasing the rate of drop of stagnation

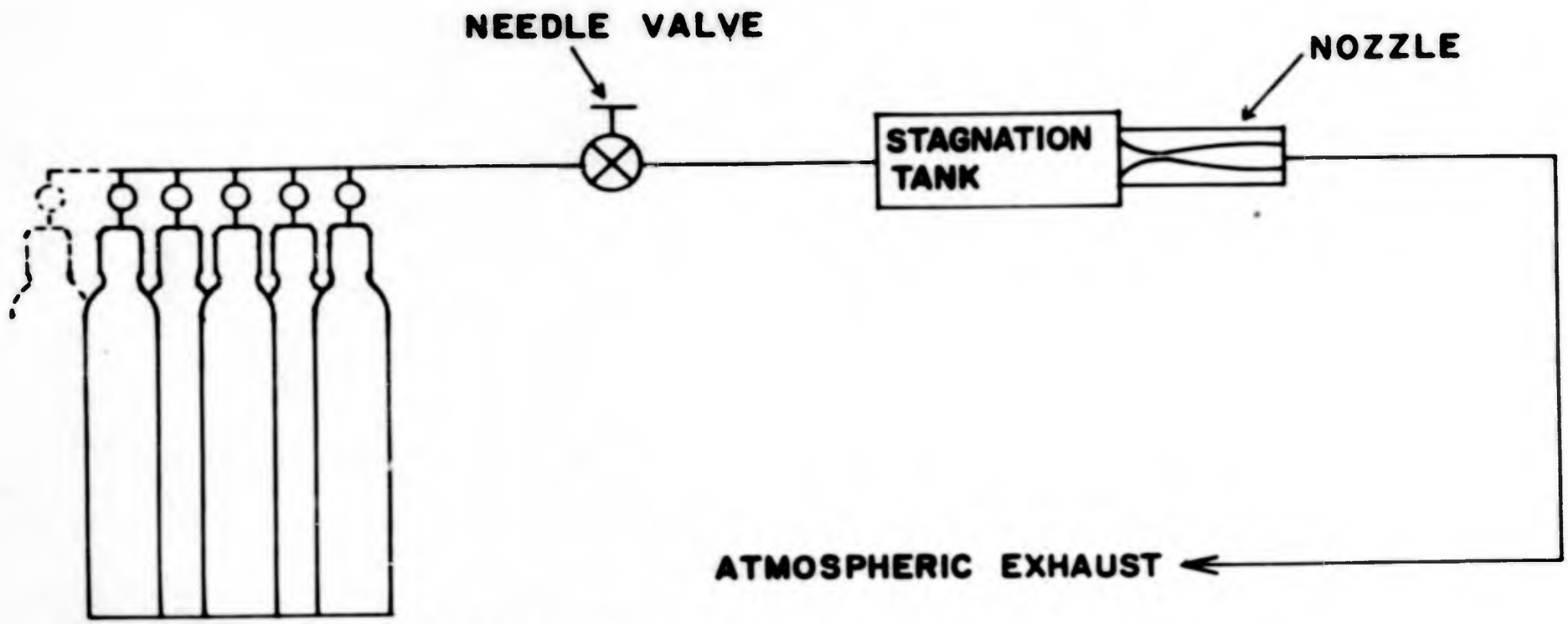

FIG 1 SCHEMATIC ARRANGEMENT OF TEST APPARATUS

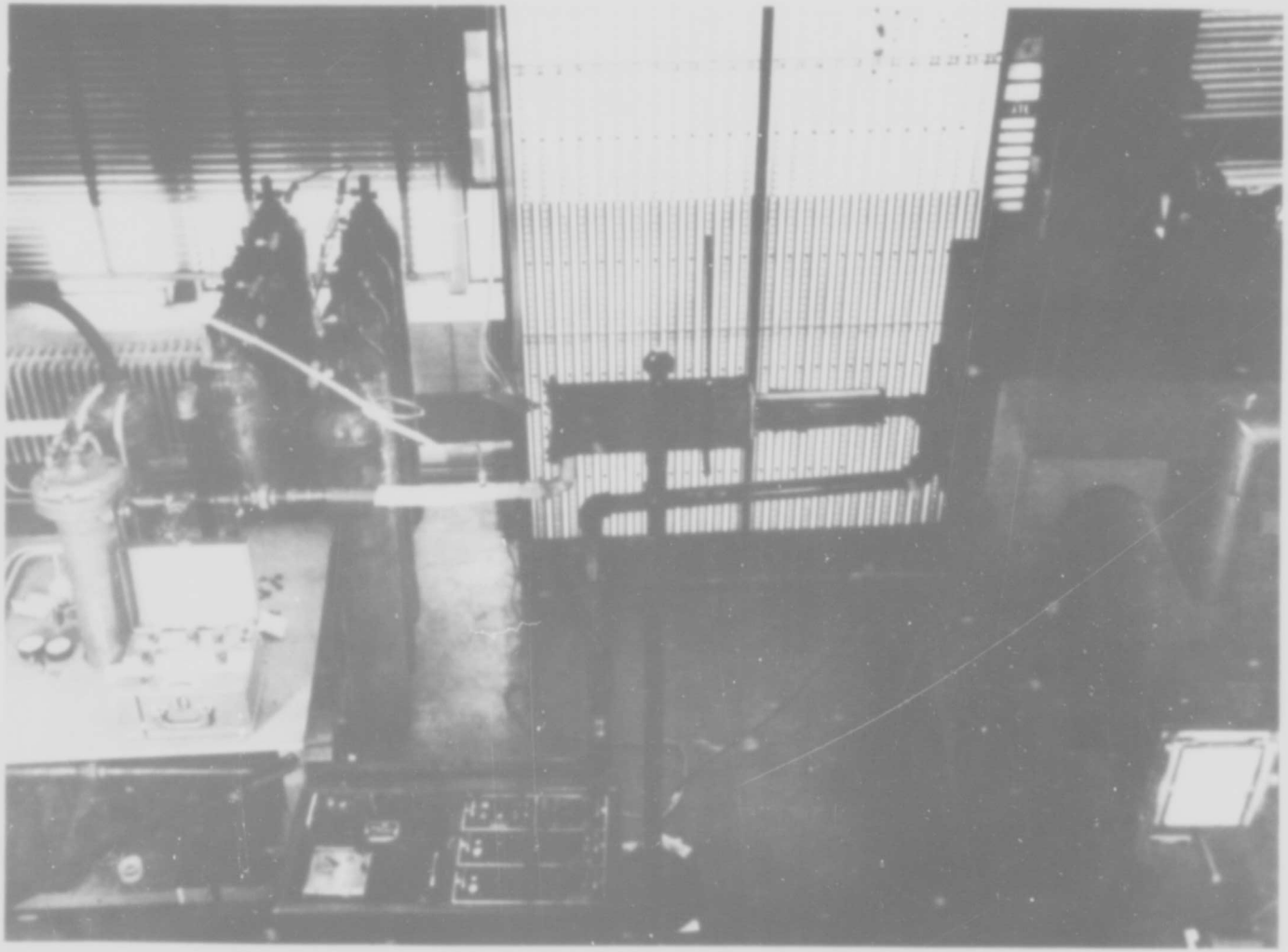

FIG 2 TEST APPARATUS

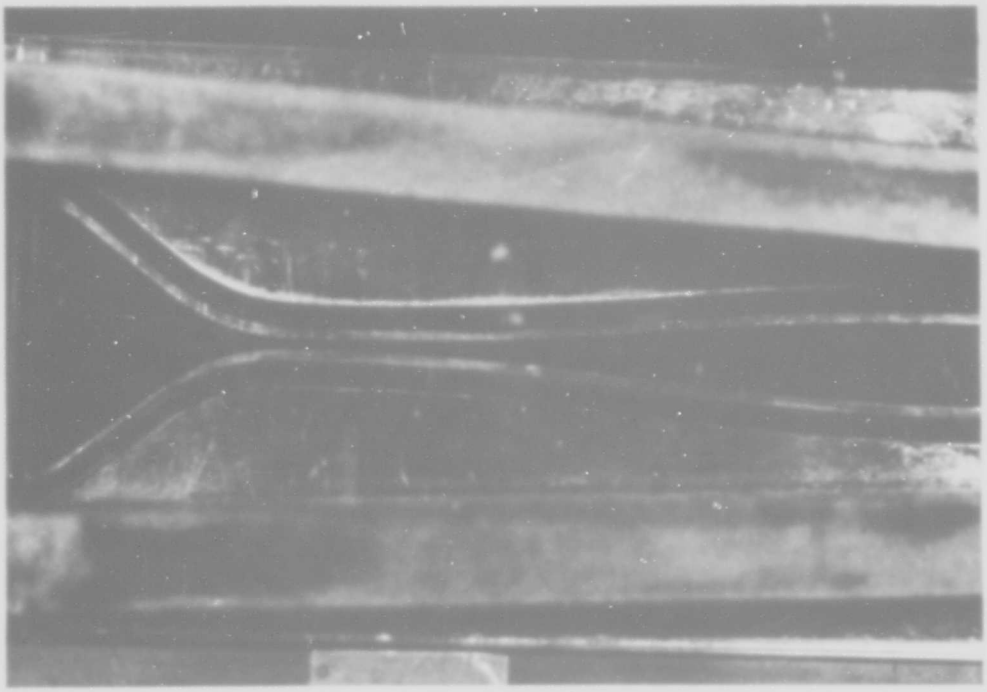

(a) no condensation

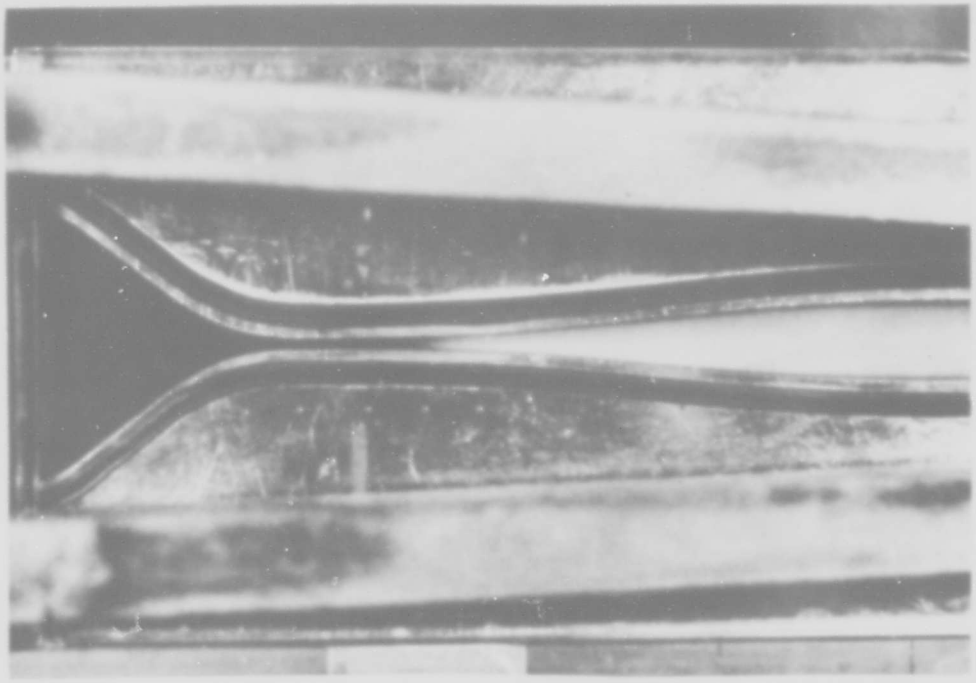

(b) condensation

FIG 4 ILLUSTRATION OF CO_2 ICE CLOUD

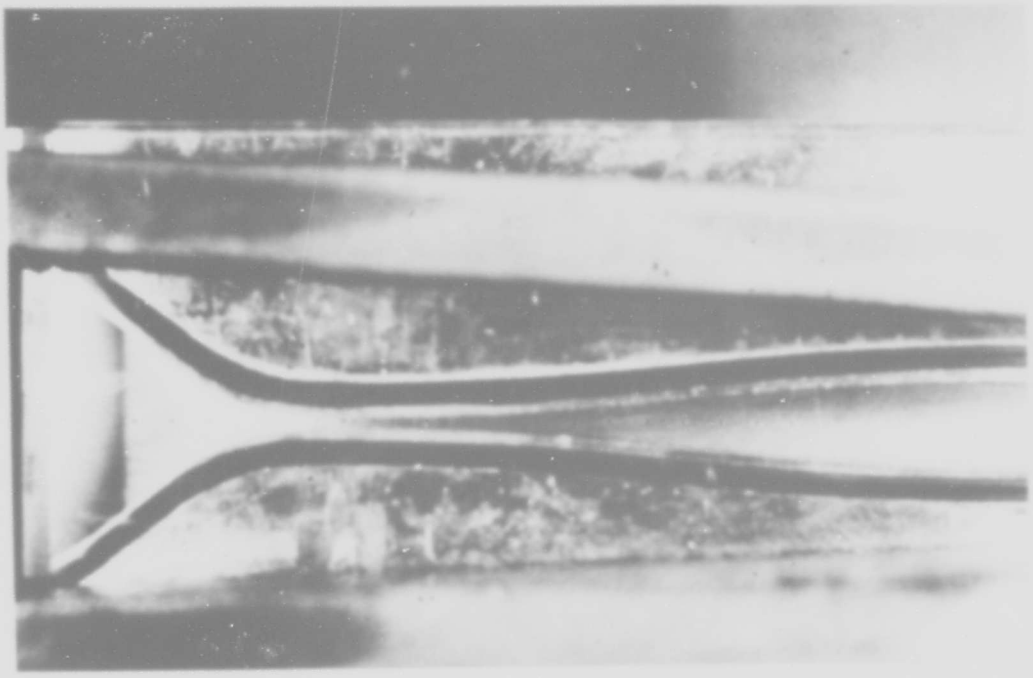

FIG 5 NOZZLE WITH PRESSURE PLATE

FIG 6 ILLUSTRATION OF MANOMETER BOARD DATA (CURVE#1)

temperature in the tank during testing. This filter was not used in any tests involving condensation included in this paper, since it was felt unnecessary in a straight blowdown of industrial CO_2, and it was desired to reduce the stagnation temperature as rapidly as possible in cases of condensation in order to conserve CO_2.

Temperature in the stagnation tank was measured with a copper-constantan thermocouple having a time constant of .6 sec. ±10%† in air of velocities comparable to those occurring in the stagnation tank. The stagnation temperature transient had a time constant which ranged from a minimum of 10 seconds to 30 seconds and more, depending on the mass flow rate. All data involving visible or evident condensation was taken after the temperature levels had become minimized, or nearly so, in order to minimize the degree of superheat in gas entering the nozzle, and hence was not influenced by transient effects. In non-condensing flow, the transient effects have undoubtedly caused some small error in temperature measurement. But as is shown in Fig. 8, temperature level had little discernible effect on the non-condensing pressure profile.

A detail arrangement of the nozzle is shown in Fig. 3. The large width to throat ratio served to minimize the boundary layer effects of the sides and hence to obtain a system of flow reasonably 2-dimensional.

The sides of the nozzle were designed to allow simple installation and removal of optical glass on each side, to be used for purposes of interferometric studies, which are further discussed later. A metal pressure plate was made identical in shape to one side of glass with pressure taps located along the nozzle plane of symmetry, and could be substituted for the glass for the purpose of gathering pressure profile data. Rubber "O-rings" in slots on each side of the nozzle prevented leakage.

† Appendix E

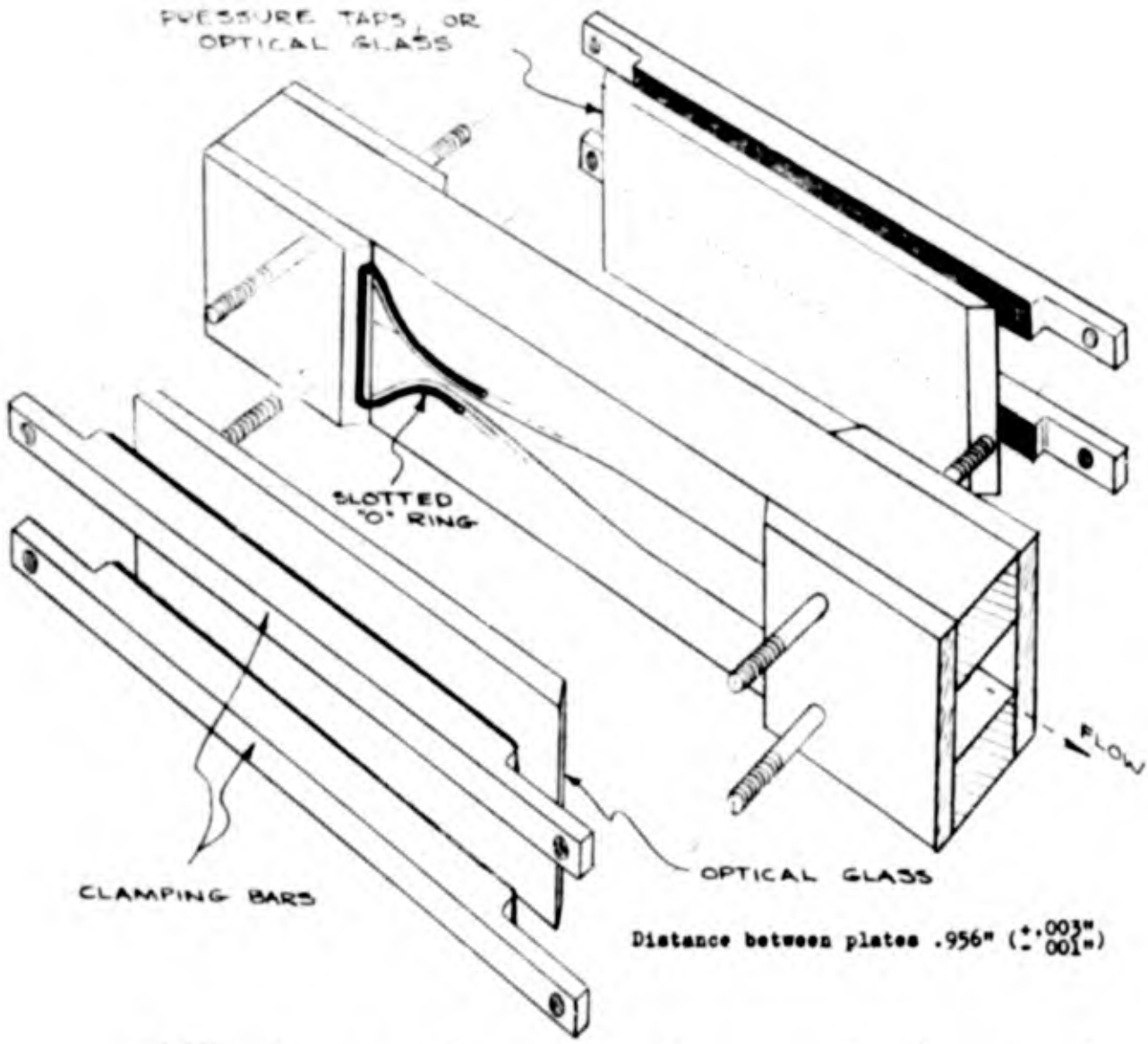

x(±.005)	b	x	b	x	b	x	b	x	b
0	1.0	1.11	.101	1.325	.055	2.07	.074	3.11	.225
.63	.550	1.15	.090	1.350	.054	2.15	.078	3.23	.250
.84	.300	1.165	.086	1.400±.015	.0531±.0001	2.21	.086	3.51	.300
.89	.250	1.190	.078	1.500	.054	2.27	.090	3.86	.358
.92	.225	1.200	.074	1.570	.055	2.38	.101	4.27	.404
.95	.200	1.220	.069	1.620	.056	2.46	.110	4.67	.428
.97	.175	1.235	.066	1.670	.057	2.52	.120	5.20	.432
1.01	.150	1.250	.063	1.735	.060	2.63	.135	on	"
1.04	.135	1.270	.060	1.820	.063	2.71	.150		
1.07	.120	1.290	.057	1.920	.066	2.84	.175		
1.09	.110	1.305	.056	1.990	.069	2.98	.200		

FIG. 3 ASSEMBLY PLAN AND OFFSETS OF TEST NOZZLE

Pressure taps were connected to a 25 tube mercury manometer board 100" in height. This facilitated measuring pressures to this level directly by manometer, accurate to .1" of mercury. Later, when it was discovered that pressure ratios upstream of and including the throat remained very nearly constant under all conditions, it was possible to disconnect taps upstream of the nozzle throat and extrapolate the throat pressure to obtain stagnation pressure. This permitted stagnation pressures of nearly 200 "Hg. A pressure gauge, accurate to 1.0 psia mounted on the stagnation tank served as a secondary, though less accurate, means of determining stagnation pressures at high pressure. Tests run ranged from 46 psia (93.3 "Hg. abs) to 112.7 psia (229 "Hg. absolute) stagnation pressure.

Data was taken by photographing the entire manometer board after steady readings of the manometers were obtained and simultaneously recording the thermocouple temperature reading. The commencement of visual condensation (the ice cloud. Fig. 4) was in most cases also measured with respect to the pressure tap holes visible through the glass.

Pressure tap holes were .016" in diameter placed .2" apart. Later, when it was discovered that more information in the vicinity of condensation would be helpful, four additional taps were added, one just upstream of the throat and three equally spaced between those already existing just downstream of the throat. These additional tap readings are included in pressure curves 3 and 4.

Photos were taken with Polaroid camera, thus expediting the processing of data. The photo for curve 1 and its accompanying data reduction table is seen in Fig. 6 and Table 1, respectively. Data for all other curves is in Appendix A.

TABLE I

Curve 1

T_o = -50.6°F

P_o = 97.5 psig ±1 psi

Barometric Pressure = 30.02"Hg.

Tube Number	Station Number	Left Side	Right Side	Total	P("Hg)	P/P_o	P/P_*
5	8 (*)	46.1	46.1	92.2	122.2	.535[1]	1.0
6	9	32.5	32.9	65.4	95.4	.417	.780
7	10	26.5	28.9	55.4	85.4	.374	.699
8	11	16.9	16.6	33.5	63.5	.278	.519
9	12	8.7	8.6	17.3	47.3	.207	.388
10	13	1.9	1.9	3.8	33.8	.147	.276
11	14	-3.7	-3.7	-7.4	22.6	.0989	.185
12	15	-6.4	-6.6	-13.0	17.0	.0744	.139
13	16	-8.5	-8.5	-17.0	13.0	.0569	.106
14	17	-9.5	-9.7	-19.2	10.8	.0473	.0884
15	18	-9.8	-10.2	-20.0	10.0	.0438	.0818
16	19	-10.3	-10.4	-20.7	9.3	.0407	.0761
17	20	-10.5	-10.6	-21.1	8.9	.0389	.0728
18	21	-10.5	-11.2	-21.7	8.3	.0363	.0678
19	22	-11.0	-11.1	-22.1	7.9	.0346	.0646
20	23	-11.3	-11.1	-22.4	7.6	.0332	.0621
21	24	-11.5	-11.7	-23.2	6.8	.0297	.0556

1) assumed

III. RESULTS OF PRESSURE MEASUREMENTS

Graphical illustrations of results obtained through pressure measurements are seen in Fig. 7(a) and 7(b). Eight curves are shown, seven involving condensation, and the eighth without condensation. The non-condensing curve is basically invariant with stagnation conditions until just prior to the compression shock, where flow becomes sub-sonic, as seen in Fig. 8. This invariancy can also be seen in the fact that a single line is common to all curves in Fig. 7 prior to condensation. Consequently, the non-condensing curve is treated as an isentropic curve based on "effective area", which is the actual area of the nozzle at any point less the effect of boundary layer displacement. No attempts to quantitatively correlate the "effective areas" resulting from non-condensing flow and those resulting from boundary layer theory are included here.

The influence of upstream conditions on the location of the condensation "shocks" is quite apparent. As one would expect, the zone of condensation moves upstream as the degree of superheat of the stagnation condition decreases. The maximum degree of stagnation superheat which produced significant condensation in the tests presented here was about 30°F. (Curve 7, Fig. 7, Curve 9, Fig. 8.) The second important effect is noted in the increased departure from the non-condensing pressure profile caused as the region of condensation approaches the throat. This is exactly what one would expect from theoretical considerations of heat addition. For the addition of heat to an ideal gas in a constant area duct:

$$\frac{dP}{P} = \frac{-kM^2}{1 - M^2} \cdot \frac{dT_o}{T}$$

The factor $(1 - M^2)$ in the denominator of the right side causes a marked increase in dP/P for a given increment of heat addition, dT_o, as M approaches 1.00. Hence, approaching the throat from the supersonic side with the

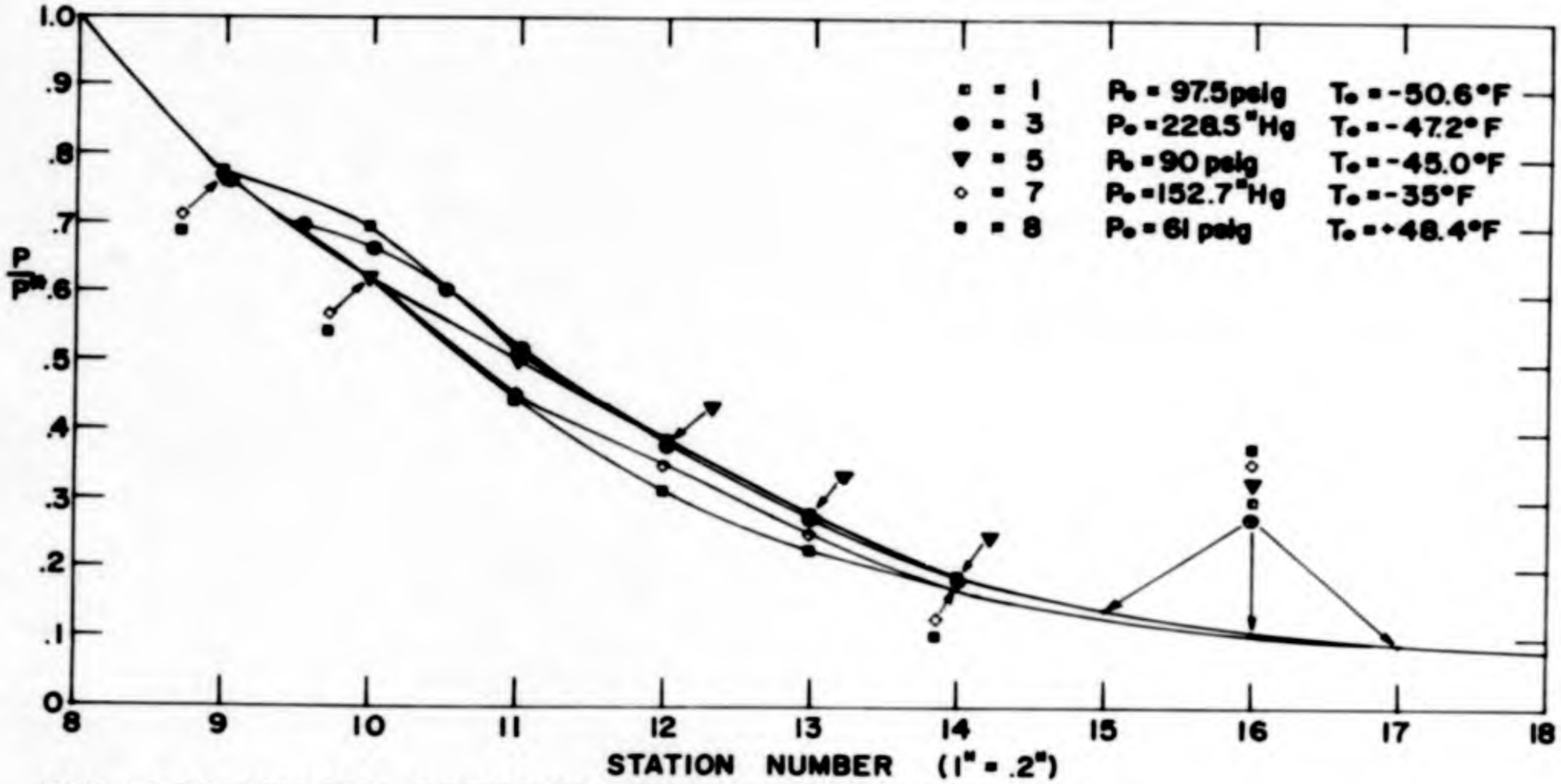

FIG 7a MEASURED PRESSURE RATIO PROFILES - CO_2

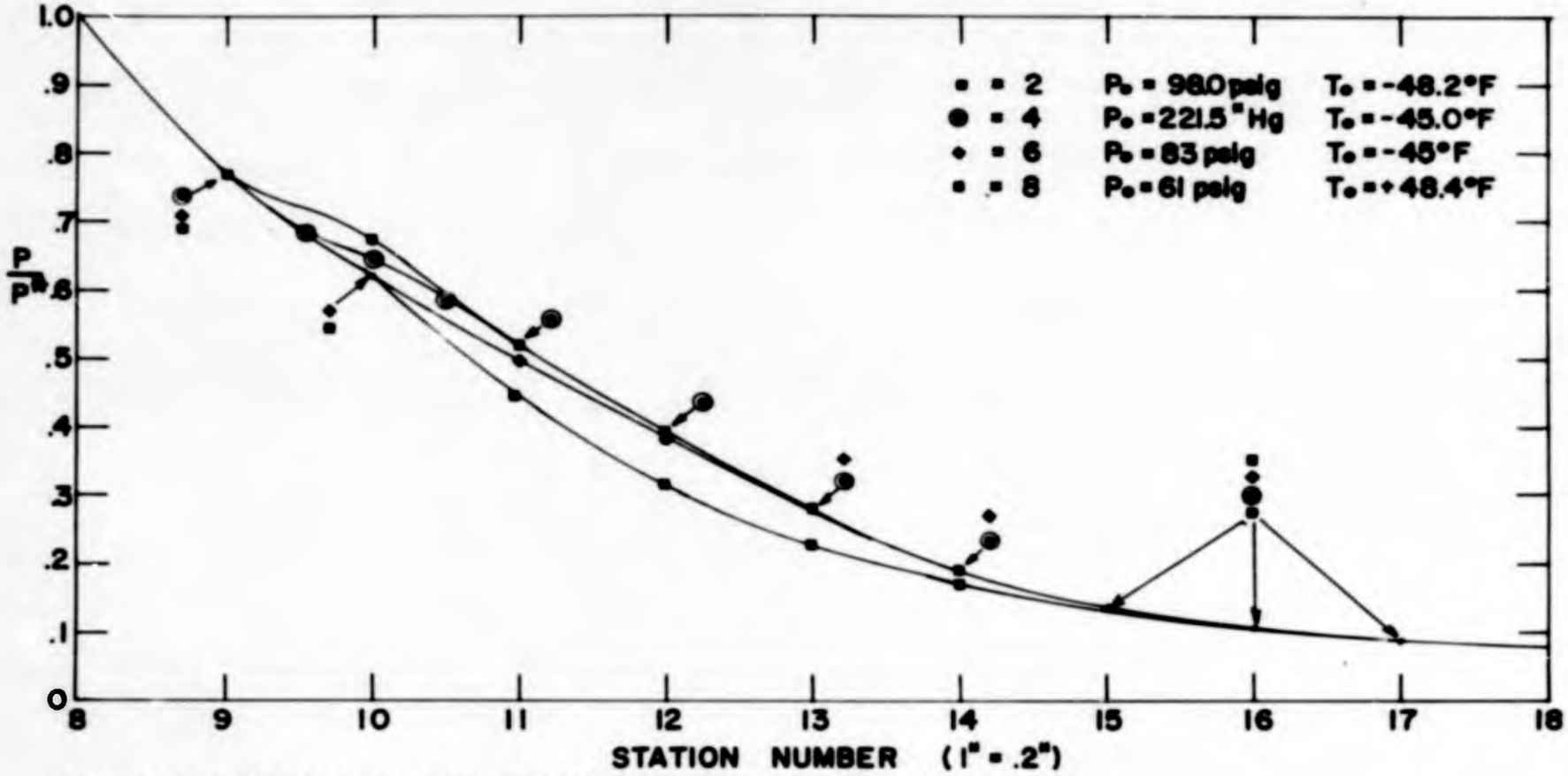

FIG 7b MEASURED PRESSURE RATIO PROFILES - CO_2

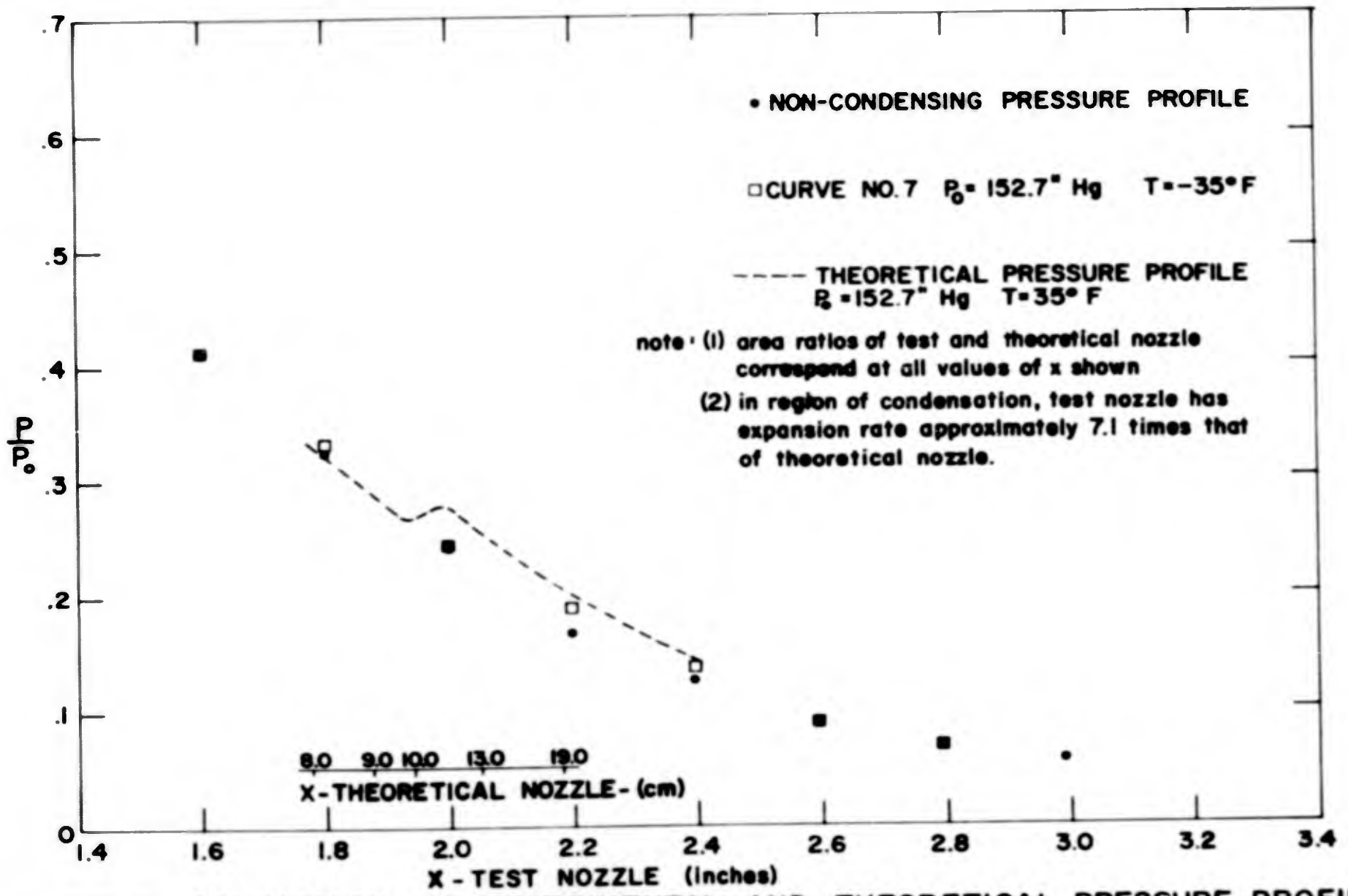

FIG 7c COMPARISON OF EXPERIMENTAL AND THEORETICAL PRESSURE PROFILES

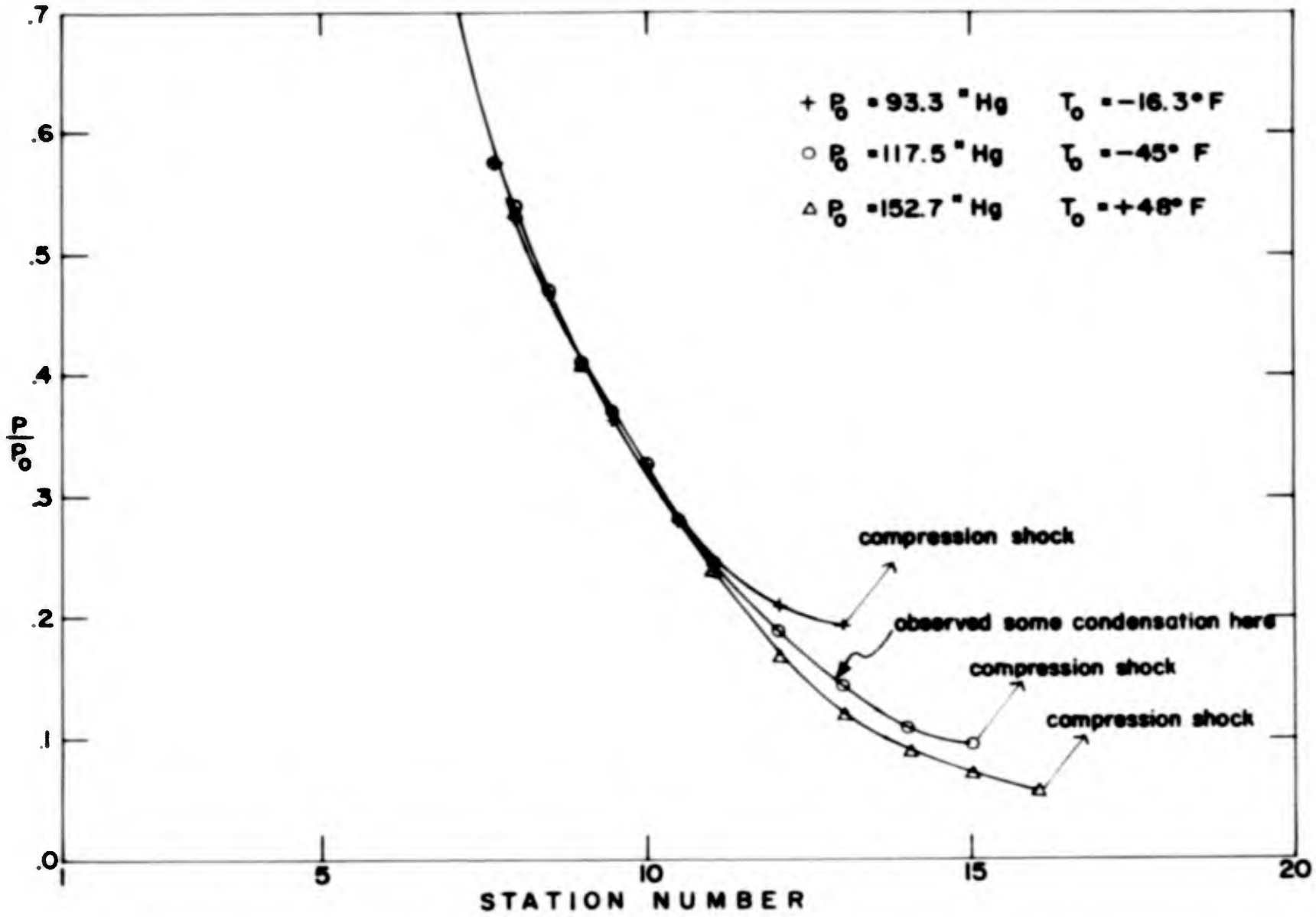

FIG. 8 EFFECT OF PRESSURE LEVEL ON NON-CONDENSING CURVES

condensation region causes progressively higher pressure "humps" in the pressure profile.

A computer program combining the theoretical treatments of Frenkel for nucleation rate, Stodola and Oswatitsch for drop growth and the gas dynamic equations has been written and is in the initial stages of testing. Presentation of the pertinent equations occurs in Appendix B.

At the time of this writing the program successfully produces a predicted pressure profile for condensing gases which do not reach such a stage of supersaturation that moisture forms upstream of the throat, and which allow a commencement of computation at $M > 1.00$. Hence, a pressure profile for the stagnation conditions existing for Curve 7, Fig. 7a has been obtained, and is shown in Fig. 7c. Unfortunately, another yet to be corrected feature of the program is its ability to consider the expansion of vapors in a variety of nozzles and the nozzle presently incorporated in the program is not the same as the test nozzle. Consequently, though the theory has condensation occurring at nearly the same area ratio (A/A^*) at which it occurs in the test nozzle, the rates of expansion of the two are entirely different. In the region of condensation the test nozzle is expanding at about 7.1 times the rate occurring in the theoretical nozzle, qualitatively explaining the lag observed in the pressure rise of the test nozzle in Fig. 7c, due to the delay in drop growth following nucleation. However, since in fact it is the area ratio (A/A^*) which is critical in determining supersaturation ratio and nucleation rate[8,9] the initial theoretical result may at least be termed encouraging.

Present intentions are to pursue all lines of this investigation and to test the predictions of theory quite comprehensively, determining the influence of the many variables involved in predicted results and their comparison with test results.

IV. INTERFEROMETER INVESTIGATIONS

General Description of the Interferometer: Extensive discussions of the theory behind interferometry techniques are numerous. References (6) and (11) are included for the reader who may desire additional detail.

Basically, an interferometer consists of a monochromatic source of light which is focused into a beam of nearly parallel rays. The beam is then split into two beams traveling separate paths of identical distance after which the beams are rejoined and focused on a viewing, or photographic plate. An interference pattern of parallel light and dark bands, as seen in Fig. 9a is formed when the two beams are rejoined due to the fact that the various rays of each beam each travel slightly different distances depending on the geometry of the mirror arrangement.

One beam is passed perpendicularly through the test section. To compensate for the change in optical path length caused by the glass side walls, "compensating" glasses of exactly the same thinkness, must be placed in the path of the other beam. During testing, the only change which occurs is the density of the vapor in the test section which influences the velocity of light passing through it according to the relation, for 2-dimensional flow:

$$\frac{S \lambda_o}{l} = n_1 - n_2$$

Where n is the index of refraction of the gas in the test section, l is the width of test section through which light passes, λ_o is the wave length of light being used, and S is the number of fringe shifts which occur at the point in question due to a change in the index from n_1 to n_2.

The index of refraction is related to the density by the relationship

$$G\rho = n - 1$$

where G is the Gladstone-Dale constant, fixed for any gas.

The technique used in this investigation was to first photograph the interference fringe pattern for no flow and then take another photograph under test conditions. The fringes of each were then numbered from a common point which effectively represented stagnation conditions. For each distance x it was then a simple, though time consuming, matter to determine the fringe shift S and thence to calculate the density ratio. Photos used in calculating the interferometer curve in Fig. 11 are shown together with a graphical illustration of the determination of S in Fig. 9a, 9c and 10, respectively. The scaling plate visible in Fig. 9b is 1.00 inches in length. The calculation table is shown in Appendix C.

Several problems have been encountered in applying the interferometer in this investigation. First, the data reduction is a time consuming process. The author has devised several steps which aid somewhat in measuring fringe locations and in arrangirg and processing the data, and the computations are easily amenable to a simple computer program. However the time required for development of negatives and prints, plus measurement of fringes does not appear readily reducible.

Second, turbulence in flow entering the nozzle increases as stagnation pressure and flow rate are increased causing the fringes upstream of the throat to become increasingly wavy and blurry until, at higher pressure they completely fade out. The acceleration of the gas and its resulting tendency to cause uniform flow results in the return to view of clear interference fringes from the vicinity of the throat downstream. The author succeeded in raising the limiting stagnation pressure at which blurring occurred from 50 to 70 psig by fabricating a streamlined cowling for introduction of the flow from the stagnation tank to the nozzle. But above this point, which is the most interesting region of investigation for CO_2, upstream fringes again became blurred. This detrimental effect, in addition to that of the

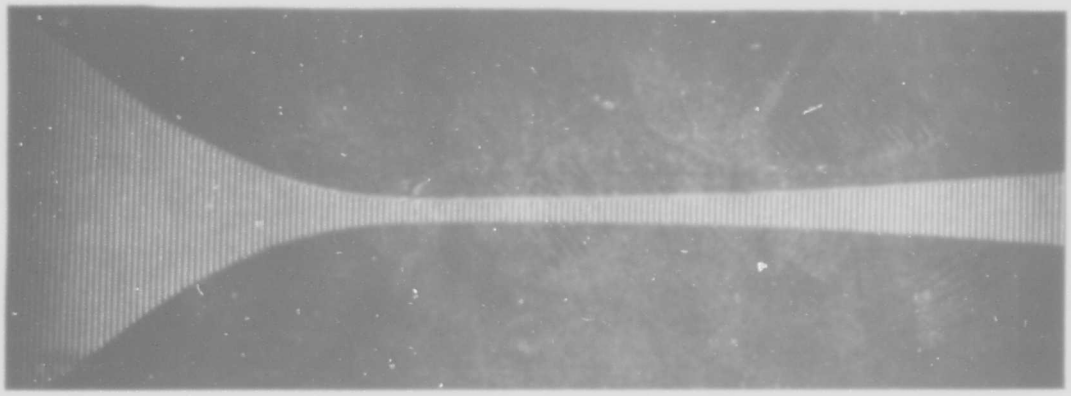

(a) no flow

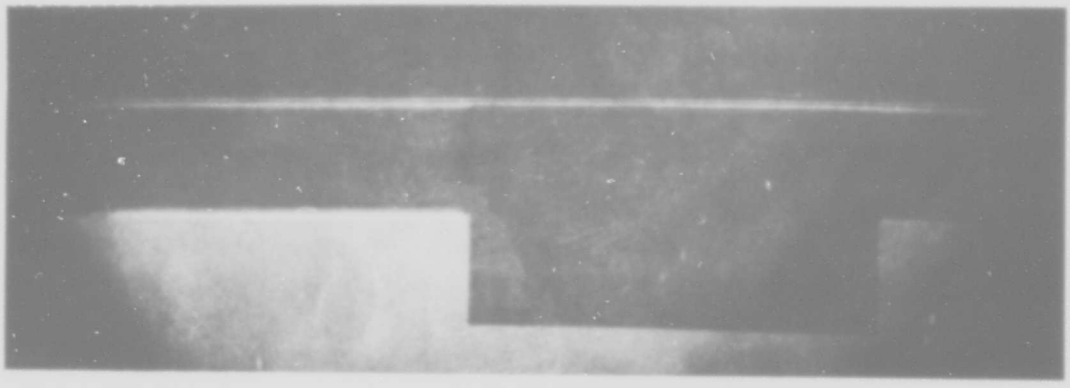

(b) scaling plate (1.00")

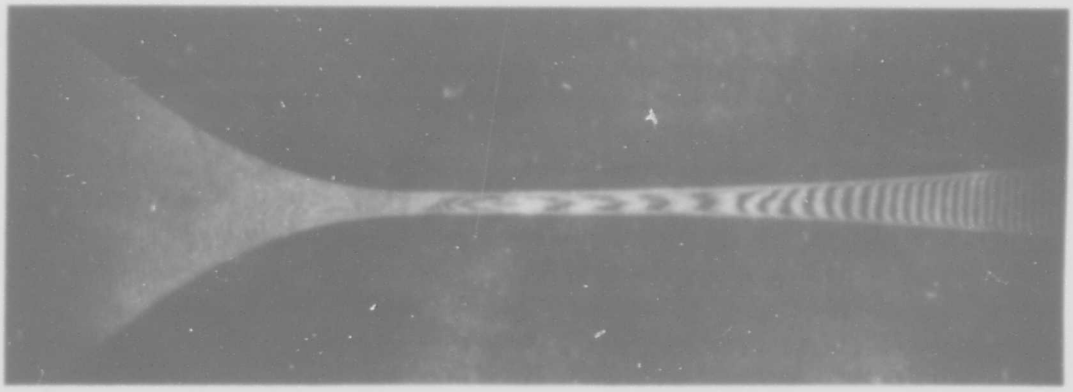

(c) flow $\{P_o = 69\,\text{psig} \pm 1\,\text{psi} \quad T_o = -9.5°F\}$

FIG 9 INTERFEROMETER PHOTOS

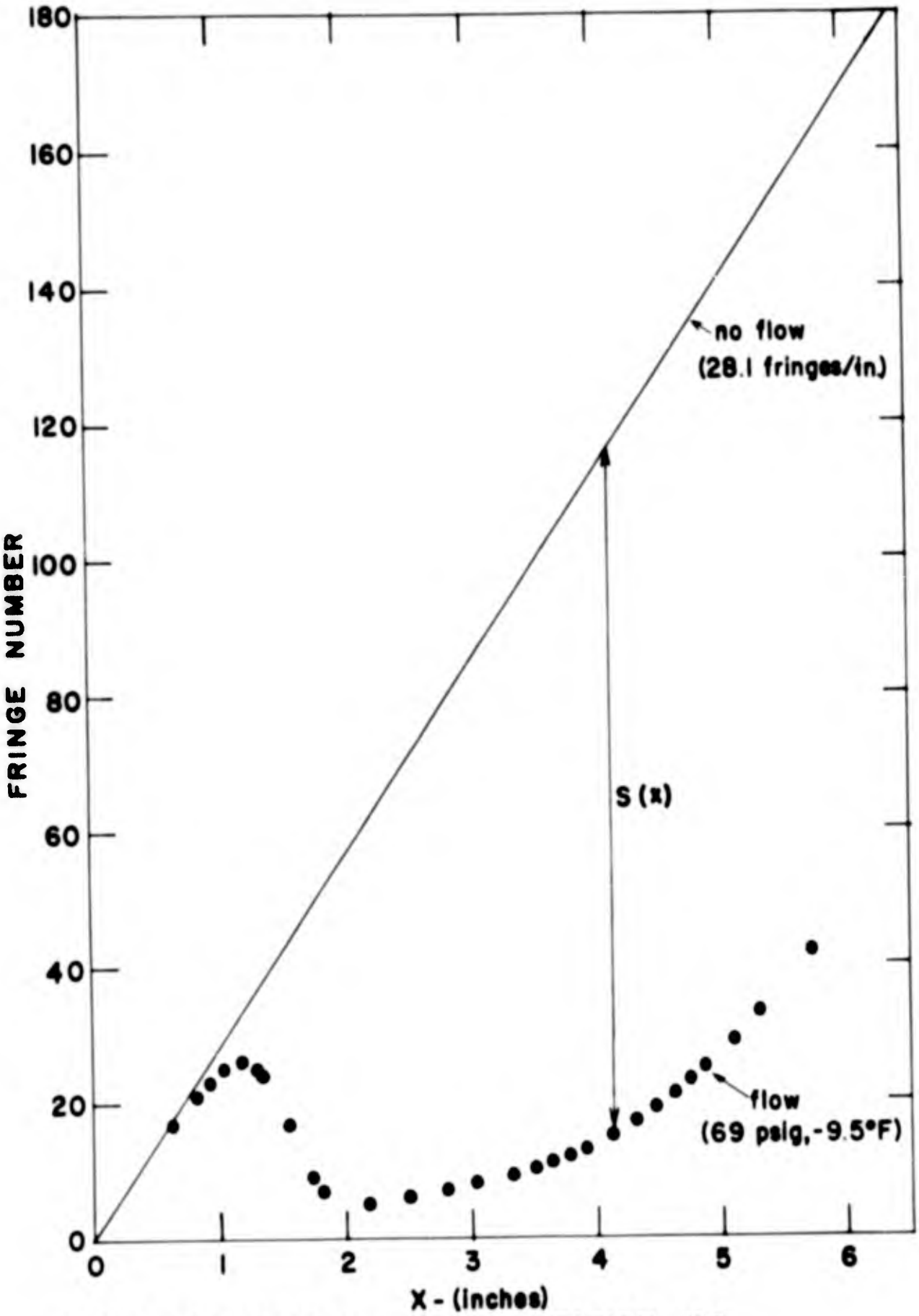

FIG 10 GRAPHICAL REPRESENTATION OF DETERMINATION OF FRINGE SHIFTS

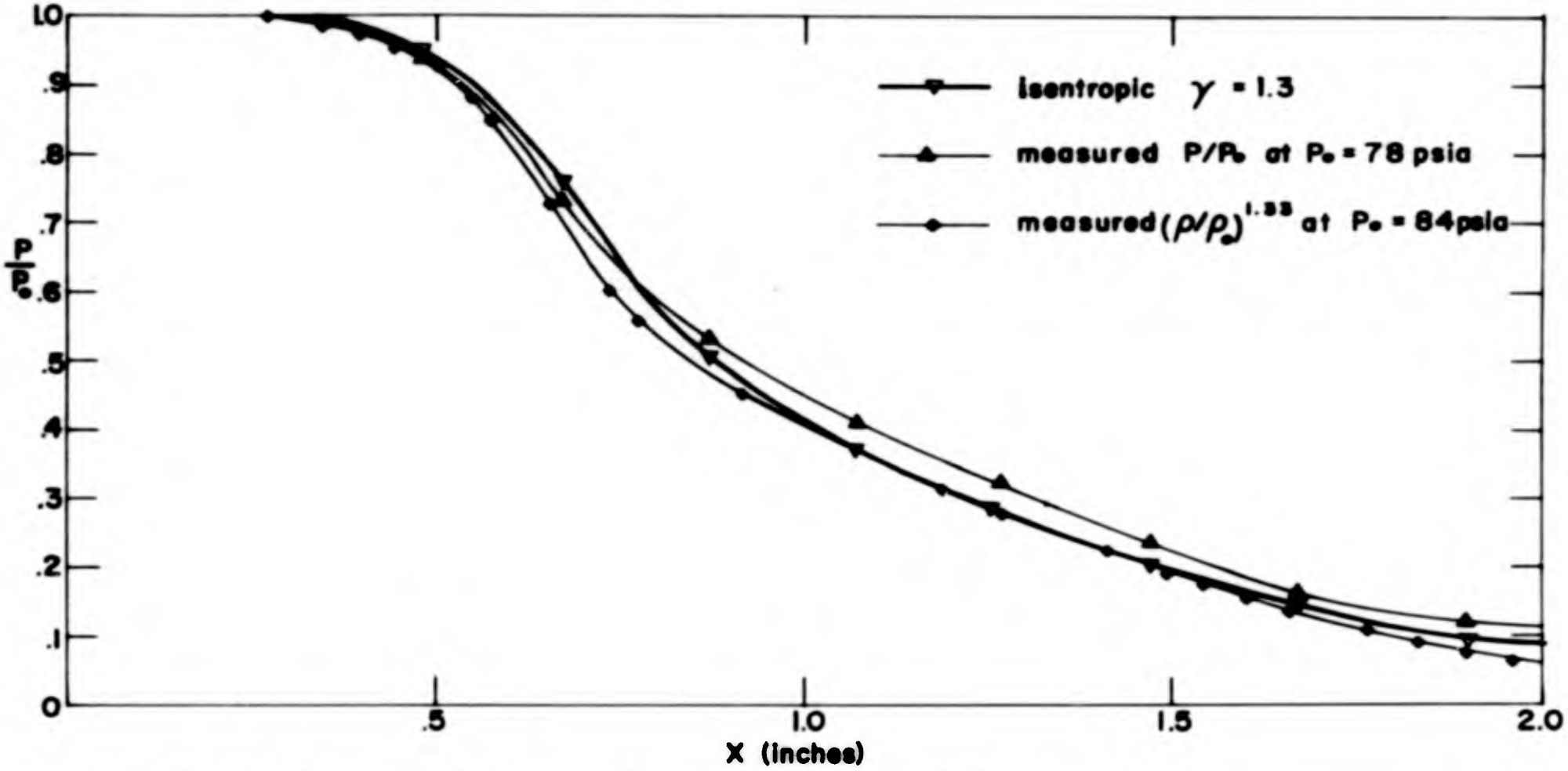

FIG II COMPARISON OF INTERFEROMETRIC AND DIRECTLY MEASURED PRESSURE PROFILES

inexperienced developing hand of the author, is clearly visible in Fig. 9c, taken at 69 psig, about the maximum pressure where upstream fringes remain visible.

Of course, if upstream conditions can be assumed, it is possible at high pressures to extrapolate to a point where the fringes come into view and then proceed as before, but clearly this would limit the desirability of the technique to some extent.

The third problem encountered is evident in Fig. 11 where the pressure profile (converted isentropically from the density ratios) from the interferometer is compared with that of the pressure taps for the non-condensing case. It is seen that the curve obtained from density measurements is lower at all points than that obtained by direct pressure measurements. At least one qualitative explanation of this is readily seen. First, temperatures upstream in the vicinity of 0°F and below result in temperatures in the supersonic section of between -150°F and -300°F. Thus, despite the relatively thin boundary layer, high velocities and heat transfer coefficients next to the wall cause temperatures and hence, densities to be considerably higher than in the main stream, though the pressures are the same. The net effect is a greater fringe shift than would occur at main stream density.

This effect of greater fringe shift can be seen in the boundary layer adjoining the top and bottom nozzle wall in Fig. 9c, and may provide an accurate means of supplying a correction to the first results by presenting information both on the boundary layer thickness and the fringe shift which takes place in this region.

V. CONCLUSIONS

Test results indicate a definite region of supersaturation of CO_2 prior to its condensation during expansion. In Curve 1, using assumed isentropic

temperatures based on measured pressure ratio, the supersaturation ratio (P/P_∞) obtains an estimated value of 9.14, prior to condensation occurring. In this expression P_∞ is the pressure at which a flat surfaced liquid would remain at equilibrium with its vapor, at the temperature of the environment.

In Curve 3, the supersaturation ratio reaches a value of 10.5 prior to condensation and in Curves 4, 5 and 7 values of 11.6, 13.4 and 16.8, respectively. Calculations of these figures are in Appendix D.

The fact that supersaturation ratios steadily increase prior to the occurence of rapid condensation tends to support the predictions of nucleation theory that, for CO_2, the lines of constant nucleation rate diverge with decreasing pressure and temperatures and that nucleation rates have a critical value of P/P_o beyond which they rise astronomically, creating a narrow zone where the large portion of condensation occurs.[8,9,21] The nucleation rates predicted by equation a(1) in Appendix B are shown in Fig. 12, and indicate that a greater supersaturation is required at lower temperatures to obtain a given nucleation rate.

However, in the absence of more complete testing of the combination of nucleation, drop growth, and gas dynamic theory, little more can be said at present.

It is further concluded that the interferometer does not lend itself to the convenient procurement of accurate density and pressure profiles in this particular nozzle under these extreme temperature conditions. The degree of accuracy in profiles obtained, however, in the absence of any corrective procedures, provides a reasonable hope that simple correction procedures can be applied to increase the interferometer's accuracy and usefulness for this study.

The fact that interference fringes in the interferometer photos remain nearly verticle at all regions of the nozzle until the boundary layer is

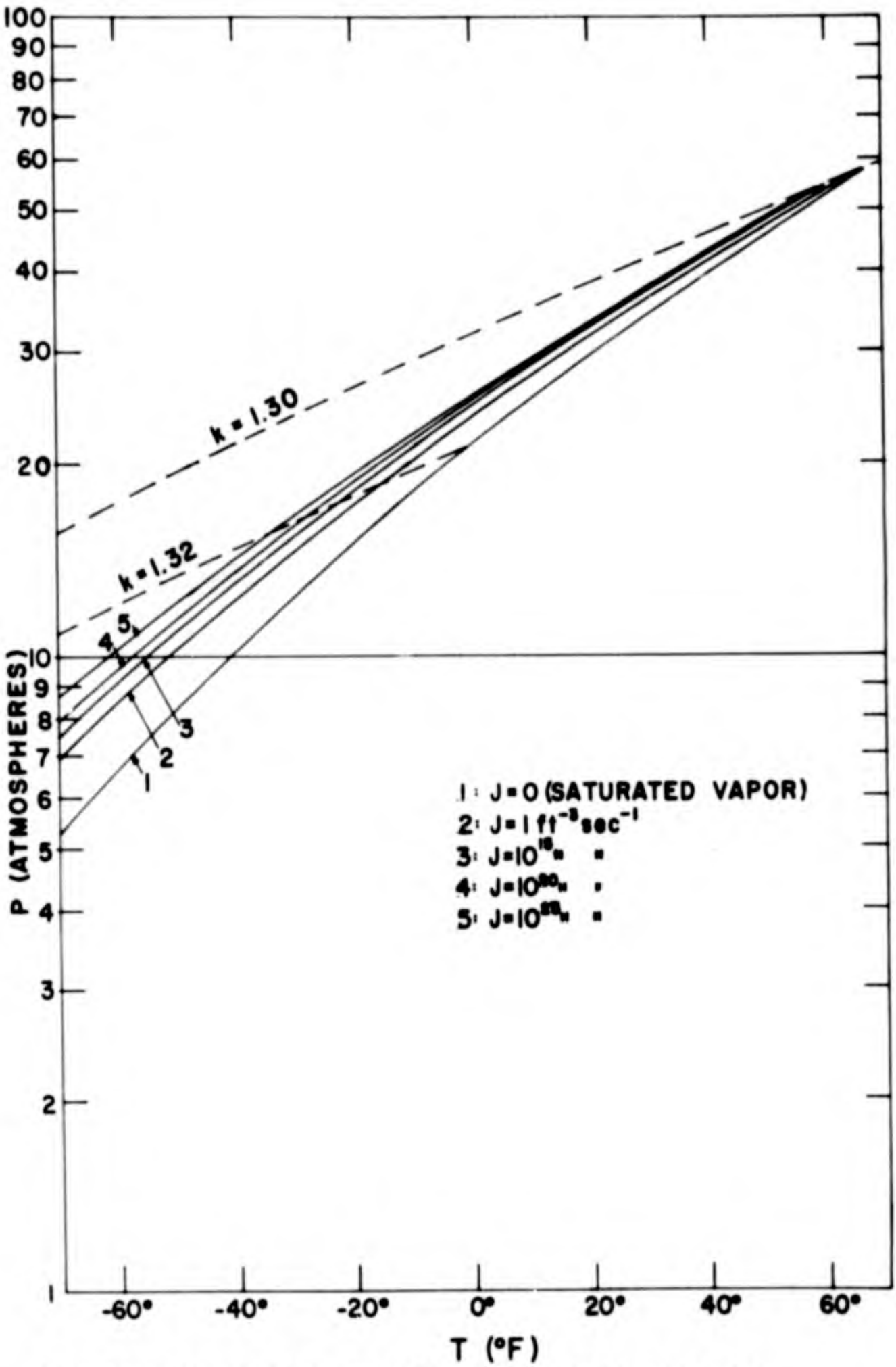

FIG 12 PREDICTED NUCLEATION RATES FOR CO_2

reached, and the observation that the boundary layer is small supports the assumption that the flow is not merely 2-dimensional, but is effectively 1-dimensional between boundary layers and justifies the use of 1-dimensional gas dynamic relations in application of the theory.

Pressure tap measurements provide a simple and sensitive means of detecting condensation in nozzles provided that the properties of the gas are such that heat released by condensation is sufficient. The critical parameter involved here is h_{fg}/C_p†, the ratio of latent heat of vaporization to the specific heat at constant pressure, a table of which is provided in Appendix F for numerous gases at room temperature. CO_2 was selected for this experimentation for its relatively higher value of h_{fg}/C_p, but the marked pressure variations recorded would suggest that similar experimentation would be useful with other gases having lesser values.

† Appendix B, Equation c (1)

BIBLIOGRAPHY

1. Barnard, A. J. - Proc. Royal Society - London - AZZO, p. 132 - 1953.

2. Becker, R. and Doring, W. - Ann. der Physics - Vol. 25, p. 719 - 1935.

3. Binnie, A. M. and Green, T. R. - Proc. Royal Society - London - Vol. 181, p. 134 - 1942.

4. Courtney, W. G. - Jour. Chemistry and Physics - Vol. 34, p. 2018 - 1962.

5. Courtney, W. G. - "Re-Examination of Nucleation and Condensation of Water" - not yet published.

6. Dean, R. C. (Defrate, L. A., Barry, F. W. and Bailey, D. Z.) - Aerodynamic Measurements - M.I.T. Gas Turbine Laboratory - 1952.

7. Faro, I., Small, T. R. and Hill, F. K. - Jour. Applied Physics - Vol. 34, p. 40 - 1952.

8. Frenkel, J. - Kinetic Theory of Liquids - Oxford Univ. Press - 1946.

9. Hill, P. W., Witting, H. and Demetri, E. P. - ASME Trans. Jour. of Heat Transfer - Nov. 1963, p. 303 - 1963.

10. Hirth, J. P. - Ann. N. Y. Academy of Science - Vol. 101, p. 805 - 1963.

11. Keenan, J. H. and Kaye, J. - Gas Tables - Wiley and Sons, Inc. - 1948.

12. Ladenburg, R., Van Voorhis, C. C. and Winckler, J. - Interferometric Study of Supersonic Phenomena - NavOrd Report 69 - 46, - 1946.

13. Lothe, J. and Pound, G. M. - Jour. Chemistry and Physics - Vol. 36, p. 2080 - 1962.

14. Matheson Company Inc. - Matheson Gas Data Book - James Grey, Inc. - 1961.

15. Oriani, R. A. and Sundquist, B. E. - Jour. Chemistry and Physics - Vol. 38, p. 2082 - 1963.

16. Oswatitsch, K. - Z. Angew. Math.und Mech. - Vol. 22, p. 1 - 1942.

17. Reiss, H. - Jour. Chemistry and Physics - Vol. 20, p. 1216 - 1952.

18. Stever, H. G. and Rathbun, K. C. - NACA TN 2559 - 1951.

19. Stodola, A. - Steam and Gas Turbines - McGraw-Hill Pub. Co. - pp. 117-128, 1034-1073 - 1927.

20. Volmer, M. and Flood, H. - Z. Phys. Chem. - Vol. A170, p. 273 - 1934.

21. Wegener, P. P. - "Condensation Phenomena in Nozzles" - AIAA Preprint No. 63-509 - 1963.

22. Wegener, P. P. and Pouring, A. A. - Physics of Fluids - Vol. 7, p. 352 - 1964.

23. Willmarth, W. W. and Nagamatsu, H. T. - Jour. Applied Physics - Vol. 23, p. 1089 - 1952.

24. Yang, W. T. - "A Study of Homogeneous Nucleation from Vapor to Droplets" Doctoral Dissertation - Yale University - 1963.

APPENDIX A.

I. POSITIONS OF PRESSURE TAPS

All locations ±.005"

Station Number	x (referred to Station 1)
1	0.0
2	.195
3	.400
4	.600
5	.795
6	1.005
7	1.205
7 1/2	1.340
8	1.400
8 1/2	1.510
9	1.610
9 1/2	1.710
10	1.805
10 1/2	1.905
11	2.005
12	2.205
13	2.405
14	2.610
15	2.800
16	3.005
17	3.200
18	3.405
19	3.605
20	3.800
21	4.000
22	4.210
23	4.410
24	4.610
25	4.805
26	5.205
27	5.600
28	6.015
29	6.410
30	6.805
31	7.205
32	7.570

APPENDIX A.

II. DATA FOR ILLUSTRATED PRESSURE CURVES

Curve 1

T_o = -50.6°F

P_o = 97.5 psig ±1 psi

Barometric Pressure = 30.02"Hg.

Tube Number	Station Number	Left Side	Right Side	Total	P("Hg)	P/P_o	P/P_*
5	8(*)	46.1	46.1	92.2	122.2	.535[1]	1.0
6	9	32.5	32.9	65.4	95.4	.417	.780
7	10	26.5	28.9	55.4	85.4	.374	.699
8	11	16.9	16.6	33.5	63.5	.278	.519
9	12	8.7	8.6	17.3	47.3	.207	.388
10	13	1.9	1.9	3.8	33.8	.147	.276
11	14	-3.7	-3.7	-7.4	22.6	.0989	.185
12	15	-6.4	-6.6	-13.0	17.0	.0744	.139
13	16	-8.5	-8.5	-17.0	13.0	.0569	.106
14	17	-9.5	-9.7	-19.2	10.8	.0473	.0884
15	18	-9.8	-10.2	-20.0	10.0	.0438	.0818
16	19	-10.3	-10.4	-20.7	9.3	.0407	.0761
17	20	-10.5	-10.6	-21.1	8.9	.0389	.0728
18	21	-10.5	-11.2	-21.7	8.3	.0363	.0678
19	22	-11.0	-11.1	-22.1	7.9	.0346	.0646
20	23	-11.3	-11.1	-22.4	7.6	.0332	.0621
21	24	-11.5	-11.7	-23.2	6.8	.0297	.0556

1) assumed

Curve 2

T_o = -48.2°F

P_o = 98.0 psig ±1 psi

Barometric Pressure = 30.02"Hg.

Tube Number	Station Number	Left Side	Right Side	Total	P("Hg)	P/P_o	P/P_*
5	8 (*)	46.3	46.4	92.7	122.7	.535[1]	1.0
6	9	32.1	32.4	64.5	94.5	.411	.770
7	10	25.4	27.7	53.1	83.1	.362	.677
8	11	17.1	16.7	33.8	63.8	.278	.520
9	12	9.0	9.0	18.0	48.0	.209	.391
10	13	2.0	2.0	4.0	34.0	.148	.277
11	14	-3.6	-3.6	-7.2	22.8	.0995	.186
12	15	-6.4	-6.6	-13.0	17.0	.0741	.1385
13	16	-8.5	-8.5	-17.0	13.0	.0567	.106
14	17	-9.5	-9.7	-19.2	10.8	.0471	.088
15	18	-9.9	-10.2	-20.1	9.9	.0431	.0806
16	19	-10.3	-10.3	-20.6	9.4	.0409	.0765
17	20	-10.4	-10.5	-20.9	9.1	.0396	.0740
18	21	-10.3	-11.0	-21.3	8.7	.0378	.0708
19	22	-10.8	-10.9	-21.7	8.3	.0361	.0675
20	23	-11.2	-11.0	-22.2	7.8	.0340	.0635
21	24	-11.4	-11.6	-23.0	7.0	.0310	.0570
22	25	-11.2	-11.5	-22.7	7.3		

1) assumed

Curve 3

T_o = -47.2°F

P_o = 228.5"Hg (calculated)

Barometric Pressure = 30.04"Hg.

Tube Number	Station Number	Left Side	Right Side	Total	P("Hg)	P/P_o	P/P_*
4	8 (*)	46.5	45.8	92.3	122.3	.535[1]	1.0
5	8 1/2	38.5	38.5	77.0	107.0	.467	.874
6	9	31.5	32.0	63.5	93.5	.409	.764
7	9 1/2	26.6	29.0	55.6	85.6	.374	.699
8	10	26.0	25.5	51.5	81.5	.356	.665
9	10 1/2	22.0	22.1	44.1	74.1	.322	.605
10	11	16.6	16.5	33.1	63.1	.275	.515
11	12	8.5	8.5	17.0	47.0	.206	.384
12	13	1.5	1.5	3.0	33.0	.144	.269
13	14	-3.9	-4.0	-7.9	22.1	.0963	.180
14	15	-6.6	-6.7	-13.3	16.7	.0730	.1364
15	16	-8.5	-8.7	-17.2	12.8	.0559	.1045
16	17	-9.5	-9.7	-19.2	10.8	.0471	.0880
17	18	-9.9	-10.1	-20.0	10.0	.0436	.0815

1) assumed

Curve 4

T_o = -45.0°F

P_o = 221.5"Hg (calculated)

Barometric Pressure = 30.04"Hg.

Tube Number	Station Number	Left Side	Right Side	Total	P("Hg)	P/P_o	P/P_*
3	7 1/2	49.8	49.2	99.0	129.0	.583	
4	8 (*)	45.1	43.3	88.4	118.4	.535[1]	1.00
5	8 1/2	37.4	37.3	74.7	104.7	.473	.884
6	9	30.2	30.6	60.8	90.8	.410	.766
7	9 1/2	24.5	26.7	51.2	81.2	.367	.685
8	10	23.4	23.0	46.4	76.4	.345	.644
9	10 1/2	19.4	19.4	38.8	68.8	.311	.588
10	11	15.4	15.2	30.6	60.6	.274	.511
11	12	8.2	8.1	16.3	46.3	.2095	.390
12	13	1.5	1.4	2.9	32.9	.149	.278
13	14	-3.9	-4.0	-7.9	22.1	.100	.186
14	15	-6.5	-6.7	-13.2	16.8	.076	.142
15	16	-8.5	-8.8	-17.3	12.7	.0574	.107
16	17	-9.7	-9.8	-19.5	10.5	.0474	.0885
17	18	-10.2	-10.4	-20.6	9.4	.0424	.0793
18	19	-10.0	-10.7	-20.7	9.3	.0420	
19	20	-10.6	-10.6	-21.2	8.8	.0398	
20	21	-10.9	-10.8	-21.7	8.3	.0375	
21	22	-11.0	-11.2	-22.2	7.8	.0352	
22	23	-11.0	-11.2	-22.2	7.8	.0352	
23	24	-10.2	-10.6	-20.8	9.2	.0416	

1) assumed

Curve 5

T_o = -45°F ±2

P_o = 90 psig ±1psi

Barometric Pressure = 29.97"Hg.

Tube Number	Station Number	Left Side	Right Side	Total	P("Hg)	P/P_o	P/P_*
5	8 (*)	41.2	41.2	82.4	112.4	.535[1]	1.0
6	9	27.8	28.2	56.0	86.0	.409	.765
7	10	19.1	20.9	40.0	70.0	.333	.622
8	11	13.3	13.0	26.3	56.3	.268	.501
9	12	7.0	6.9	13.9	43.9	.2085	.390
10	13	0.9	0.9	1.8	31.8	.151	.282
11	14	-4.2	-4.3	-8.5	21.5	.102	.191
12	15	-6.6	-6.8	-13.4	16.6	.0778	.1453
13	16	-8.7	-8.7	-17.4	12.6	.0599	.1120
14	17	-9.7	-9.9	-19.6	10.4	.0495	.0925
15	18	-10.1	-10.4	-20.5	9.5	.0452	.0844
16	19	-10.5	-10.6	-21.1	8.9	.0424	.0793
17	20	-10.6	-10.8	-21.4	8.6	.0409	.0765
18	21	-10.4	-11.2	-21.6	8.4	.0400	.0748
19	22	-10.7	-10.7	-21.4	8.6	.0409	.0765

1) assumed

Curve 6

T_o = -45°F ±2°F

P_o = 83 psig ±1 psi

Barometric Pressure = 29.97"Hg.

Tube Number	Station Number	Left Side	Right Side	Total	P("Hg)	P/P_o	P/P_*
5	8 (*)	37.9	37.9	75.8	105.8	.535[1]	1.0
6	9	25.2	25.6	50.8	80.8	.408	.764
7	10	16.7	18.4	35.1	65.1	.329	.615
8	11	11.4	11.1	22.5	52.5	.266	.497
9	12	5.4	5.2	10.6	40.6	.2055	.384
10	13	-0.3	-0.3	-0.6	29.4	.149	.279
11	14	-5.0	-5.1	-10.1	19.9	.101	.189
12	15	-7.2	-7.4	-14.6	15.4	.0778	.1453
13	16	-9.0	-9.1	-18.1	11.9	.0602	.1125
14	17	-10.0	-10.1	-20.1	9.9	.0501	.0936
15	18	-10.2	-10.5	-20.7	9.3	.0470	.0878
16	19	-10.5	-10.6	-21.1	8.9	.0450	.0841
17	20	-10.5	-10.7	-21.2	8.8	.0445	.0832
18	21	-10.0	-10.7	-20.7	9.3	.0470	.0878
19	22	-10.1	-10.1	-20.2	9.8	.0495	.0925

1) assumed

Curve 7

T_o = -35°F ±5°F

P_o = 152.7"Hg. (calculated)

Barometric Pressure = 30.2"Hg.

Tube Number	Station Number	Left Side	Right Side	Total	P("Hg)	P/P_o	P/P_*
5	8 (*)	25.7	25.7	51.4	81.6	.535[1]	1.0
6	9	16.0	16.4	32.4	62.6	.410	.767
7	10	9.7	10.8	20.5	50.7	.332	.621
8	11	3.4	3.4	6.8	37.0	.2425	.453
9	12	-0.7	-0.7	-1.4	28.8	.189	.353
10	13	-4.7	-4.5	-9.2	21.0	.138	.257
11	14	-8.2	-8.2	-16.4	13.8	.0904	.169
12	15	-9.7	-9.8	-19.5	10.7	.0701	.131
13	16	-10.9	-10.9	-21.8	8.4	.0551	.103
14	17	-9.7	-9.7	-19.4	10.8	.0708	.132
15	18	-8.9	-9.1	-18.0	12.2	.0800	.149
16	19	-9.0	-9.0	-18.0	12.2	.0800	
17	20	-8.3	-8.3	-16.6	13.6	.0892	
18	21	-6.0	-6.4	-12.4	17.8	.117	
19	22	-4.3	-4.2	-8.5	21.7	.142	
20	23	-3.0	-2.9	-5.9	24.3	.159	
21	24	-2.9	-2.8	-5.7	24.5	.161	
22	25	-3.6	-3.7	-7.3	22.9	.150	
23	26	-3.9	-4.0	-7.9	22.3	.146	
24	27	-3.4	-3.4	-6.8	23.4	.153	

1)assumed

Curve 8

T_o = +48.4°F

P_o = 61 psig ±1 psi

Barometric Pressure = 30.04"Hg.

Tube Number	Station Number	Left Side	Right Side	Total	P("Hg)	P/P_o	P/P_*
5	8 (*)	25.8	25.8	51.6	81.6	.535[1]	1.0
6	9	16.1	16.3	32.4	62.4	.409	.765
7	10	9.5	10.5	20.0	50.0	.327	.611
8	11	3.2	3.1	6.3	36.3	.238	.445
9	12	-2.2	-2.2	-4.4	25.6	.168	.314
10	13	-5.7	-5.6	-11.3	18.7	.1226	.229
11	14	-8.0	-8.1	-16.1	13.9	.0911	.170
12	15	-9.4	-9.5	-18.9	11.1	.0727	.136
13	16	-10.5	-10.5	-21.0	9.0	.0590	.111
14	17	-9.4	-9.5	-18.9	11.1	.0727	.136
15	18	-8.9	-9.1	-18.0	12.0	.0786	.147
16	19	-8.8	-8.8	-17.6	12.4	.0812	.152

1) assumed

Curve 9

T_o = -45.0°F

P_o = 117.5"Hg.

Barometric Pressure = 30.04"Hg.

Tube Number	Station Number	Left Side	Right Side	Total	P("Hg)	P/P_o
1	1	43.3	44.2	87.5	117.5	1.0
2	7	28.6	28.2	56.8	86.8	.738
3	7 1/2	19.5	19.0	38.5	68.5	.583
4	8 (*)	17.1	16.6	33.7	63.7	.542
5	8 1/2	12.7	12.7	25.4	55.4	.471
6	9	9.2	9.4	18.6	48.6	.413
7	9 1/2	6.2	6.8	13.0	43.0	.366
8	10	4.2	4.0	8.2	38.2	.325
9	10 1/2	1.5	1.5	3.0	33.0	.281
10	11	-.7	-.7	-1.4	28.6	.243
11	12	-3.7	-3.8	-7.5	22.5	.191
12	13	-6.2	-6.5	-12.7	17.3	.147
13	14	-8.6	-8.7	-17.3	12.7	.108
14	15	-9.2	-9.4	-18.6	11.4	.097

Curve 10

T_o = -16.3°F

P_o = 93.3"Hg.

Barometric Pressure = 30.04"Hg.

Tube Number	Station Number	Left Side	Right Side	Total	P("Hg)	P/P_o
1	1	31.3	32.0	63.3	93.3	1.0
2	7	19.4	19.2	38.6	68.6	.735
3	7 1/2	12.1	11.7	23.8	53.8	.576
4	8 (*)	9.9	9.6	19.5	49.5	.531
5	8 1/2	6.5	6.5	13.0	43.0	.461
6	9	4.0	4.0	8.0	38.0	.407
7	9 1/2	1.6	2.0	3.6	33.6	.360
8	10	.1	.1	.2	30.2	.324
9	10 1/2	-1.7	-1.8	-3.5	26.5	.284
10	11	-3.7	-3.7	-7.4	22.6	.242
11	12	-5.1	-5.2	-10.3	19.7	.211
12	13	-5.8	-6.1	-11.9	18.1	.194

APPENDIX B. BASIC NUCLEATION, DROP GROWTH AND GAS DYNAMICS EQUATIONS

Following are the theoretical equations being used in the effort to determine the predictions of theory referred to in the text. The drop growth equations are developed along the lines used by Stodola[19] and Oswatitsch,[16] which considers incident and evaporating molecules, plus drop temperature and the necessary mass and energy equations. The only change in development has been to employ 2RT as the expression for average energy per unit mass of flux to and from the drop surface, rather than 3RT/2, which is the average energy of all the vapor particles. The nucleation rate equation is that of Frenkel[8] and does not include any of the many possible modifying features which more recent authors have suggested.[1,4,5,10,13,15]

a) Nucleation Rate:

$$1)\quad J = \left(\frac{P}{KT}\right)^2 \cdot \frac{m}{\rho}\sqrt{\frac{2\sigma}{\pi m}}\ \exp\left(\frac{-4\pi\sigma r^{*2}}{3KT}\right)$$

where r* is the Kelvin-Helmhotz critical radius, at which a liquid drop is in equilibrium with its vapor.

b) Drop Growth:

$$1)\quad \frac{\xi}{2RT}\left[U_{fg} + \frac{1}{2}RT_D\right]\left[1 - \frac{P_\infty}{P}\exp\left\{\frac{2\sigma}{\rho RT_D}\right\}\left(\frac{T}{T_D}\right)^{\frac{1}{2}}\right] = \frac{T_D}{T} - 1$$

$$2)\quad \frac{dr}{dt} = -\frac{2P}{\rho\sqrt{2\pi RT}}\left[\frac{RT_D - RT}{U_{fg} + \frac{1}{2}RT_D}\right]$$

Equation (1) is used to determine drop temperature, T_D, and (2) to determine drop growth rate.

c) Gas Dynamics Equations:

$$1)\quad \frac{dp}{dx} = P \cdot \frac{kM^2}{M^2 - 1}\left[\left(\frac{h_{fg}}{C_p T} - \frac{1}{1-\mu}\right)\frac{d\mu}{dx} - \frac{1}{A}\frac{dA}{dx}\right]$$

$$2)\quad \frac{dV}{dx} = -\frac{V}{kM^2}\cdot\frac{1}{P}\frac{dp}{dx}$$

$$3)\quad \frac{dT}{dx} = T\cdot\left(\frac{k-1}{k}\right)\cdot\frac{1}{P}\frac{dp}{dx} + \frac{h_{fg}}{C_p}\frac{d\mu}{dx}$$

The computation program referred to in the text involves a sequence of small step changes, Δx, taken along the nozzle, at each point of which calculations based on the above equations are made. Changes in (μ) are based on the nucleation and drop growth equations.

The problem incurred in passing through the throat when moisture is forming ($\frac{d\mu}{dx} \neq 0$) is apparent when $M \to 1$ in equation C (1) above.

More complete testing and comparison of theoretical predictions will follow in a later publication.

APPENDIX C. CALCULATION TABLE--INTERFEROMETER DATA

T_o = -9.5°F

P_o = 69.0 psig ±1 psi

No Flow: Average 28.1 fringes/inch

$$\frac{\lambda}{l} = \frac{5461 \times 10^{-8}}{(.956)(2.54)} = 2248 \times 10^{-8}$$

Photograph Scale: 2.35 in./in.

$$\rho_o = \frac{P}{RT} = \frac{(83.7)(144)(44)}{(1545)(450)} = .763 \text{ lbm/ft}^3$$

$$G\rho_o = N_o - 1 = (.3673 \times 10^{-2})(.763) = 280.2 \times 10^{-5}$$

1	2	3	4	5	6	7	8
Fringe Number	x_{photo}	S(x)	$\frac{S\lambda}{l} \times 10^5$	$(n_o-1)-(4)$	ρ/ρ_o	x_{nozzle}	$(\rho/\rho_o)^{1.33}$
0	0	0	0				
1	.035						
9	.335	0	0				
17	.630	.46	1.035	279.2	.996	.268	.995
21	.810	1.45	3.26	276.9	.988	.345	.984
23	.920	2.50	5.62	274.6	.980	.392	.974
25	1.040	3.82	8.59	271.6	.965	.442	.954
26	1.180	6.8	15.3	264.9	.945	.502	.928
25	1.300	11.1	25.0	254.2	.907	.552	.878
24	1.350	13.5	30.4	249.8	.880	.574	.844
17	1.550	26.2	58.9	221.3	.789	.659	.730
9	1.730	39.2	88.2	192.0	.685	.735	.604
7	1.820	43.8	98.6	181.6	.648	.774	.562
5	2.180	56.0	126.0	154.2	.550	.918	.452
6	2.510	64.4	145.0	135.2	.482	1.067	.379
7	2.805	71.8	161.8	118.4	.421	1.192	.316
8	3.030	77.1	173.6	106.6	.380	1.289	.276
9	3.315	84.1	189.3	90.9	.324	1.410	.224
10	3.510	88.6	199.5	80.7	.288	1.492	.191
11	3.630	91.0	204.8	75.4	.269	1.545	.174
12	3.765	94.0	211.5	68.7	.245	1.602	.154
13	3.900	96.7	217.7	62.5	.223	1.660	.136
15	4.120	101.0	226.3	53.9	.192	1.753	.111
17	4.310	104.2	234.6	45.6	.163	1.833	.090
19	4.460	106.5	239.8	40.4	.144	1.899	.076
21	4.610	108.7	244.5	35.7	.127	1.960	.0644
23	4.740	110.4	248.6	31.6	.113	2.018	.0550
25	4.860	111.7	251.3	28.9	.103	2.067	.0486
29	5.09	114.2	257.2	23.0	.0785	2.165	.0340
33	5.30	116.1	261.5	18.7	.0667	2.253	.0273
42	5.72	119.0	267.8	12.4	.0442	2.453	.0162

APPENDIX D. SUPERSATURATION RATIOS

Curve 1 $T_o = -50.6°F$

$P/P_* = .790$ $P_* = 122.2$ $P_t/P_o = .535$

$P/P_o = .423$ $(T/T_o) = (.423)^{\frac{.33}{1.33}} = .8065$

$T = .8065(409.0) = 330.0°R\ (-129.6°)$

at $-129.6°F$, $P_{sat} = 5.20$ psia

$$P/P_\infty = \frac{(122.2)(.790)}{(5.20)(2.03)} = 9.14$$

Curve 3

$P/P_* = .710$ $P_* = 122.3$ "Hg.

$P/P_o = .380$ $T/T_o = .785$

$T = .785(415) = 326°R\ \ (-134°F)$

at $-134°F$, $P_{sat} = 4.05$ psi

$$P/P_\infty = \frac{(122.3)(.710)}{(4.05)(2.03)} = 10.53$$

Curve 4

$P/P_* = .680$ $P/P_o = .363$

$T = .776(414.6) = 322°R\ (-138°F)$

at $-138°F$, $P_{sat} = 3.4$ psia

$$P/P_\infty = \frac{(118.4)(.680)}{(3.4)\ (2.03)} = 11.63$$

Curve 5

$P/P_* = .630$ $P/P_o = .337$

$T/T_o = (.337)^{.25} = .762$ $T = .762(415) = 316°R\ \ (-144°F)$

at $-144°F$, $P_{sat} = 2.6$ psia

$$P/P_\infty = \frac{(122.4)(.630)}{(2.6)\ (2.03)} = 13.4$$

Curve 7

$T_o = -35°$

$P/P_* = .460$

$P_* = 81.6$ "Hg.

$P/P_o = .246$

$T/T_o = (.246)^{.25} = (.704)$

$T = .704(425) = 299°R$ $(-161°F)$

at $-161°F$, $P_{sat} = 1.10$ psia

$$P/P_\infty = \frac{(81.6)(.460)}{(1.10)(2.03)} = 16.8$$

APPENDIX E. ESTIMATION OF EXPERIMENTAL ERROR

TEMPERATURE MEASUREMENTS

Estimated error (difference between measured and actual temperature) on temperature readings except where otherwise noted is +0.5°, -2.5°F. This was determined after the following measurements and observations.

1. Temperature of various portions of the ice bath of the reference junction were found to vary by as much as +2°F from the freezing point, 32.2°F, despite its containment in an insulated thermos.
2. A calibration of the potentiometer (Wheatstone bridge type) used for measurements, compared exactly with those readings of the standard copper-constantan conversion tables at each end (32°F and 212°F) of the calibration and showed a maximum variation of +1.0°F between.
3. The time constant of the thermocouple was measured with the aid of a Sanborn Recorder capable of recording a 50 cps signal with no distortion. Subjecting the thermocouple to various changes of temperature, it was found that for still water τ = .15 sec, for still air, τ = 1.4 sec, and for response to the variation of human breath, τ = .6 sec. The measured time constant of the potentiometer was .9 sec $\pm$.2 sec.

Based on these observations, a reference temperature of 32.2°F was assumed for all measurements and the variation in ice bath temperature allowed for in the estimated larger possible negative error.

Assuming a linear temperature transient over a 30 second period, a variation from 80°F to -50°F would result in a rate change of -4.33°F/sec. Hence, for the non-condensing curves, this effect alone could contribute an error of about 5°F, in the thermocouple (τ = .6) and potentiometer circuit (τ = .9 sec). Hence, in the non-condensing curves, an error of +4.5°F, -2.5°F is estimated. In measurements involving condensation, care was taken to let temperature readings reach a relatively constant level before data (photos) were taken. No transient effects are estimated for these cases.

PRESSURE

Pressure readings taken by the mercury manometer board are estimated accurate within ±.1 "Hg. Since the lowest pressures recorded on these curves range around 8 "Hg., this would amount to ±1.25% error in the pressure ratios near station 18 on the charts.

In the region of condensation (station 10) pressure levels range near 80 "Hg. Hence error in pressure ratios in this region is estimated at ±.125%, two orders of magnitude less than the pressure variation caused by condensation at this point.

Error has been introduced into the values of stagnation pressure wherever they have not been directly measured by the manometer board owing to the high pressure level. General observations of the behavior of the pressure ratio at the throat have shown that although its value remained remarkably close to .535 for all pressure levels, it had a slight tendency to decrease with increasing pressure. Based on these observations (and others with air, where average P/P_o measured .523 and the same tendence was noted) it is estimated that the pressure ratio at the throat could have been lowered to a minimum value of .525 at the highest pressure levels. Hence, calculated stagnation pressures are estimated to have an error of +1%, -2%. For curve 1, this would amount to a variation of 4.2 "Hg., or 2 psi, which is greater than the estimated error in the pressure gauge used on the stagnation tank. However, any reduction in the estimated -2% maximum error in calculated stagnation pressures would be purely arbitrary.

In the calculation of experimental supersaturation ratios, the effects of the uncertainty in measurements may be seen by recalculating that value of supersaturation reached in curve 1 under properties varied by the possible error.

$T_o = -50.6°F + 2.5°F = -48.1°F$

$P/P_* = .790$ $\qquad P_t = 122.2$

$P/P_o = (.790)(.525) = .415$

$T/T_o = (.415)^{\frac{.33}{1.33}} = .8028$ $\qquad T = (.8028)(411.5) = 330.5$

$P_{sat} = 5.35$ psia $\qquad P/P_\infty = \frac{(122.2)(.790)}{(5.35)(2.03)} = \underline{\underline{8.86}}$

This compares with the value of 9.14 obtained under the measured conditions. It is seen that the uncertainty in stagnation pressure is much less important than the uncertainty in temperature. Also, the accuracy of P_{sat} for a given T is important.

Any calculation involving the ratio of specific heats, k, involves some error due to the fact that this factor is of non-constant value during the expansion. By Keenan and Kaye's Gas Tables[11] k = 1.298 at 40°F, 1.331 at -60°F, and 1.369 at -160°F. For this reason an average value of k = 1.33 has been applied to determination of temperature ratios and supersaturation ratios. This same use of k for all x in the conversion of interferogram density ratios to pressure ratios has contributed some small error to the larger experimental error previously noted.

APPENDIX F. VAPORS PROPERTIES

FLUID	(h_{fg}) Lat. Heat of Vap.	C_p Specific Heat	h_{fg}/C_p	T_s 1 atm
C_2H_6O (Ethyl Al.)	406 BTU/lbm	.342 BTU/lbm °F	1.19×10^3	173 °F
CH_4O (Methyl Al.)	482 BTU/lbm	.295 BTU/lbm °F	1.63×10^3	152 °F
H_2O	840 BTU/lbm	.445 BTU/lbm °F	1.89×10^3	212 °F
C_6H_6 (Benzene)	172 BTU/lbm	.280 BTU/lbm °F	6.15×10^2	175.3 °F
$CHCl_2F$ (Genetran 21)	140.15 BTU/lbm	.140 BTU/lbm °F	1.01×10^3	48 °F
NH_3 (Ammonia)	589.4 BTU/lbm	.523 BTU/lbm °F	1.12×10^3	-28 °F
BCl_3 (Boron Chloride)	68.8 BTU/lbm	.127 BTU/lbm °F	5.4×10^2	54.5 °F
Butene-1	168 BTU/lbm	.382 BTU/lbm °F	4.4×10^2	20.7 °F
Butene-2	179 BTU/lbm	.375 BTU/lbm °F	4.78×10^2	38.7 °F
CO_2	247 BTU/lbm	.198 BTU/lbm °F	1.24×10^3	-109.3 °F
Freon-22	100 BTU/lbm	.152 BTU/lbm °F	6.6×10^2	-41 °F
Difluoroethylene	276 BTU/lbm	.224 BTU/lbm °F	1.23×10^3	-117 °F
Dimethylamine	252 BTU/lbm	.374 BTU/lbm °F	6.74×10^2	44.4 °F
Ethyl Chloride	164 BTU/lbm	.244 BTU/lbm °F	6.74×10^2	54.3 °F
Ethylene Oxide	250 BTU/lbm	.268 BTU/lbm °F	9.31×10^2	51.3 °F
Isobutane	158 BTU/lbm	.355 BTU/lbm °F	4.46×10^2	10.9 °F
Methyl Acetylene	234 BTU/lbm	.357 BTU/lbm °F	6.55×10^2	-9.6 °F
Monethylamine	260 BTU/lbm	.330 BTU/lbm °F	7.87×10^2	61.8 °F
Monmethylamine	358 BTU/lbm	.320 BTU/lbm °F	1.12×10^3	20.6 °F
SO_2	171 BTU/lbm	.117 BTU/lbm °F	1.45×10^3	14 °F
Freon-11	78.3 BTU/lbm	.135 BTU/lbm °F	5.8×10^2	74.8 °F